Real-Time Dark-Field Scattering Microscopic Monitoring of the *in Situ* Growth of Single Ag@Hg Nanoalloys

Yue Liu[†,§] and Cheng Zhi Huang[†,‡,*]

[†]Education Ministry Key Laboratory on Luminescence and Real-Time Analysis, College of Chemistry and Chemical Engineering, Southwest University, Chongqing 400715, China and [‡]College of Pharmaceutical Sciences, Southwest University, Chongqing 400715, China. [§]Present address: Department of Chemistry, College of Pharmaceutical Sciences, Third Military Medical University, Chongqing 400038, China.

ABSTRACT A comprehensive understanding of the growth mechanism of nanoalloys is beneficial in designing and synthesizing nanoalloys with precisely tailored properties to extend their applications. Herein, we present the investigation in this aspect by real-time monitoring of the *in situ* growth of single Ag@Hg nanoalloys, through direct amalgamation of Ag nanoparticles with elemental mercury, by dark-field scattering microscopy. Four typically shaped Ag nanoparticles, such as rods, triangular bipyramids, cubes, and spheres, were used as seeds for studying the growth of Ag@Hg nanoalloys. The scattered light of Ag nanoparticles of different shapes, on exposure to the growth solution, exhibited a noticeable blue-shift followed by a red-shift, suggesting the growth of Ag@Hg nanoalloys. The formation of Ag@Hg nanoalloys was confirmed by scanning electron microscopy, high-resolution transmit electron microscopy, X-ray diffraction, energy-dispersive X-ray spectroscopy, and elemental mapping and line scanning. Further analysis of the time-dependent spectral data and morphological change of single nanoparticles during the growth led to the visual identification of the growth mechanism of single Ag@Hg nanoalloys. Three important steps were involved: first, rapid adsorption of Hg atoms onto Ag nanoparticles; second, initial diffusion of Hg atoms into Ag nanoparticles, rounding or shortening the particles; third, further diffusion of Hg atoms leading to the formation of spherical Ag@Hg nanoalloys. On the basis of these results, Ag@Hg nanoalloys with given optical properties can be synthesized. Moreover, dark-field scattering microscopy is expected to be a powerful tool used for real-time monitoring of the *in situ* growth of other metal nanoparticles.

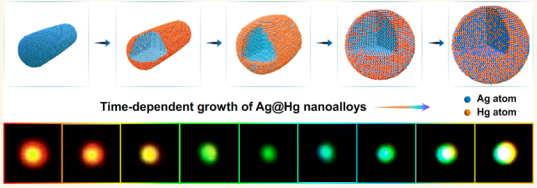

KEYWORDS: Ag@Hg nanoalloys · growth mechanism · real-time monitoring · single nanoparticles · light scattering

Nanoalloys, consisting of two or more metal elements, are of great interest, as they display significantly different structures and optical and catalytic properties from those of the pure elemental nanoparticles.[1,2] Practical applications require nanoalloys with well-defined structures and specific properties for designing new devices on a nanometric scale. Therefore, it is fundamentally important to explore the growth process of nanoalloys because the understanding of the growth mechanism allows synthesizing nanoalloys with precisely tailored properties. However, the growth mechanism of nanoalloys has rarely been studied before. Amalgams, as typical and traditional nanoalloys, have been known for centuries. However, they have rarely been used for industrial and research applications except as dental filling materials.[3] Recently, advances in nanoscale science and technology provide opportunities for amalgams to find new applications in several fields. Metal nanoparticles were employed as smart scavengers for removing mercury from polluted water[4−8] and used as optical probes for ultrasensitive Hg^{2+} detection[9−13] through the formation of amalgams. The aforementioned study included the method of the formation of amalgams; however, the growth of amalgams was not clearly understood. Further investigation of the growth process of amalgams could promote the efficiency of scavengers and enhance the detection sensitivity for Hg^{2+}. Therefore, in this study, Ag@Hg amalgams were selected as a model to investigate the growth process of nanoalloys.

Techniques employed for monitoring of the growth of nanoparticles mainly include small-angle X-ray scattering (SAXS),[14−19] time-resolved X-ray diffraction (XRD),[20] atomic force microscopy (AFM),[21−23] and liquid cell transmission electron microscopy

* Address correspondence to chengzhi@swu.edu.cn.

Received for review September 6, 2013 and accepted November 26, 2013.

Published online November 26, 2013
10.1021/nn404694e

© 2013 American Chemical Society

(TEM).[24−28] In practice, SAXS and XRD were often performed by sequentially measuring the signals of an ensemble of nanoparticles to reveal the whole growth process; however, both techniques can hardly provide direct growth information by measuring the signals of an ensemble of rather than single nanoparticles. Therefore, development of techniques to monitor the growth of single nanoparticles is critical. In this regard, AFM is a powerful tool to fulfill this task by providing 3D surface profiles of single nanoparticles. However, AFM is not a real-time method in real meaning because it always performs intermittently by disturbing the growth for image taking followed by subsequent growth, and this process was repeated several times to observe the consecutive growth of single nanoparticles.[22] In this case, the sampling process significantly interrupts the reaction, and the important phenomenon of intermediate growth is not observed. Moreover, it is difficult to relocate the same nanoparticles after the imaged sample is removed from the microscope. Recently developed liquid cell TEM has been proven as a useful tool for real-time monitoring of the *in situ* growth of single nanoparticles. However, the instrument is too expensive to afford this technique in common laboratories. In this regard, an alternative method is urgently required.

The localized surface plasmon resonance (LSPR) optical properties of noble metal nanoparticles, dramatically affected by particle parameters, such as composition, shape, size, and surrounding medium,[2,29−32] undergoes continuous changes during the growth process,[33] and the advent of dark-field scattering microscopy enables observing the dynamic changes in LSPR scattered light of single nanoparticles using a common dark-field optical microscope.[34,35] Therefore, it is reasonable to explore the growth mechanism of single nanoalloys by real-time monitoring of the LSPR changes during growth. Moreover, the optical methods used for real-time monitoring of *in situ* growth of nanoalloys at the single-nanoparticle level have not been reported.

Herein, in this study, dark-field scattering microscopy was employed for real-time monitoring of the *in situ* growth of single Ag@Hg nanoalloys, produced by direct amalgamation of Ag nanoparticles with elemental mercury (Hg^0). Ag nanoparticles of different shapes such as rods, triangular bipyramids, cubes, and spheres were used as growth seeds. The formation of Ag@Hg nanoalloys was confirmed by multiple characterizations including scanning electron microscopy (SEM), high-resolution transmission electron microscopy (HRTEM), XRD, and energy-dispersive X-ray spectroscopy (EDXS). During the growth process, the LSPR scattered light of single Ag nanoparticles exhibited a blue-shift and decrease in intensity followed by a red-shift and increase in intensity. The growth of single Ag@Hg nanoalloys underwent the following stages: first, rapid adsorption of Hg atoms onto Ag nanoparticles; second, initial diffusion of Hg atoms into Ag nanoparticles, rounding or shortening the Ag nanoparticles; third, further diffusion of Hg atoms, generating spherical Ag@Hg nanoalloys.

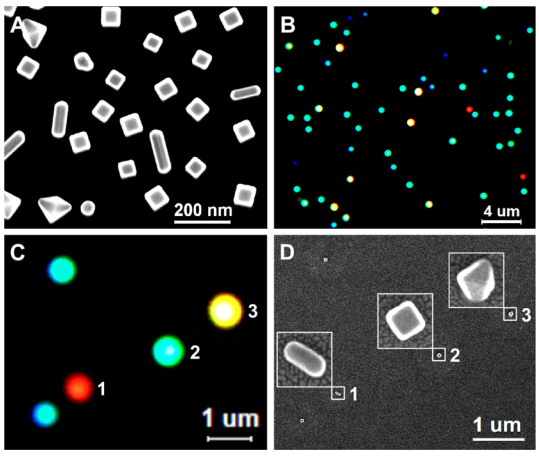

Figure 1. Characterization of Ag nanoparticles. (A) SEM image and (B) dark-field light scattering image of the prepared Ag nanoparticles. (C) Dark-field light scattering and (D) SEM images of the same collection of Ag nanoparticles. The insets in D are the enlarged SEM images of the numbered particles.

RESULTS AND DISCUSSION

Characterization of Ag Nanoparticles. Shape-controlled Ag nanoparticles scattering colorful light were synthesized following the protocol[36] described by Xia *et al.* Figure 1A displays that the prepared Ag nanoparticles had four typical shapes, namely, spheres, cubes, triangular bipyramids, and rods. Due to the inhomogeneous particle shapes and sizes, the prepared Ag nanoparticles scattered colorful light, such as blue, cyan, yellow, and red, as shown in Figure 1B. To directly determine the shapes of Ag nanoparticles by dark-field optical microscopy, we attempted to combine dark-field microscopy with electron microscopy to observe the same single Ag nanoparticles. The results showed that Ag nanoparticles scattering red, yellow, cyan, and blue light were rods, triangular bipyramids, cubes, and spheres, respectively (Figures 1C,D and S1), the same observations as in our previous work.[37] These results enabled us to directly determine the nanoparticle shapes using a dark-field optical microscope instead of expensive and complicated electron microscope. Moreover, the determination of shape by a dark-field microscope simplifies the following study of real-time monitoring of the growth of Ag@Hg nanoalloys by using Ag nanoparticles of different shapes as growth seeds. Thus, in the following experiments, we directly assigned the Ag nanoparticles scattering red, yellow, cyan, and blue light to Ag nanorods, triangular nanobipyramids, nanocubes, and nanospheres, respectively. For more information about the LSPR optical properties of the prepared Ag nanoparticles, see our previous work.[37]

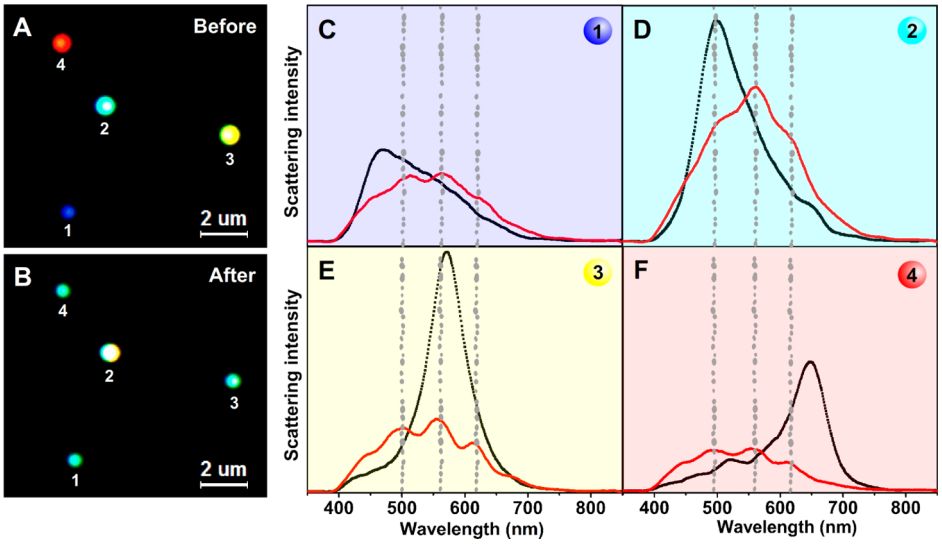

Figure 2. Characterization of four typically shaped Ag nanoparticles before and after interaction with Hg^0 by dark-field scattering microscopy and spectroscopy. (A, B) Representative dark-field light scattering images and (C−F) corresponding resonant scattering spectra of four typical Ag nanoparticles (particles 1−4) before (A, black curves) and after (B, red curves) their exposure to growth solution for 5 min. Dashed lines are drawn to facilitate the identification of peak wavelengths of the red spectra.

Interaction of Ag Nanoparticles with Hg^0. Similar to the Au−Hg system,[38] Ag@Hg nanoalloys can be produced through the diffusion of Hg atoms into Ag nanoparticles[39] because of a low cohesive energy of 0.69 eV for Hg compared to 2.95 eV for Ag.[40] Thus, in this study, Ag@Hg nanoalloys were grown by direct exposure of Ag nanoparticles to liquid Hg^0 generated by reducing Hg^{2+} with ascorbic acid.[9,41] After incubation for 5 min, the scattered light of differently shaped Ag nanoparticles exhibited significant changes (Figure S2). In general, the scattered light of single Ag nanoparticles turned cyan-green with some nanoparticles scattering strong white light due to overexposure. In addition, a few particles disappeared after incubation as they departed from the glass surface, whereas some particles appeared, attributed to the formation of nanoparticles scattering stronger light than initial Ag nanoparticles. The aforementioned four typically shaped Ag nanoparticles were selected to further discuss the light scattering changes after growth. Single Ag nanoparticles scattering blue, cyan, yellow, and red light (Figure 2A) were nanospheres (particle 1), nanocubes (particle 2), triangular nanobipyramids (particle 3), and nanorods (particle 4), with characterized scattering bands appearing at 460, 500, 570, and 640 nm, respectively (black curves, Figure 2C−F). After incubation for 5 min, the scattered light of the Ag nanorod, triangular nanobipyramid, and nanosphere turned cyan-green, whereas the Ag nanocube scattered strong white light (Figure 2B). Single particles' spectral data demonstrated that different particles after growth had similar scattering spectral profiles characterized at about 500, 560, and 615 nm with different scattered light intensities (red curves, Figure 2C−F), suggesting that the formed nanoparticles had similar composition and shape, but different sizes.

The scattering spectra of single Au nanorods in ascorbic acid solution first exhibited a blue-shift due to electron injection followed by a red-shift back to initial wavelength.[42] In this study, ascorbic acid was present in excessive amount in the growth solution. However, the effect of ascorbic acid (Figure S3) was insignificant compared to Hg^0 and thus ignored. In addition, it was believed that Hg^{2+} ions were completely reduced to form Hg^0 because the existence of free Hg^{2+} consumed Ag nanoparticles (Figure S4) due to the following oxidation reaction: $Ag^0 + Hg^{2+} \rightarrow Ag^+ + Hg^0$.[43] Thus, the observed changes in scattered light property of single Ag nanoparticles were due to Hg^0, which led to the change in particle parameters. Taken together, the changes in LSPR scattering properties were attributed to the diffusion of Hg^0 into Ag nanoparticles and formation of Ag@Hg nanoalloys, thus changing the composition, shape, and size of the Ag nanoparticles.[41]

Characterization of Ag@Hg Nanoalloys. SEM, HRTEM, XRD, EDXS, and elemental mapping and line scanning were used to characterize the morphology, lattice, and composition of Ag nanoparticles before and after growth to confirm the formation of Ag@Hg nanoalloys. Ag nanoparticles had specific shapes such as rod, cube, and triangular bipyramid before growth (Figure 3A); however, only spheres were observed after growth (Figures 3B and S5). The formed nanoparticles had similar parameters, which explains the similar scattering spectral profiles of differently shaped Ag nanoparticles after growth. Two key aspects of the shape transformation are as follows. First, the amalgamation took place more efficiently and preferentially on the

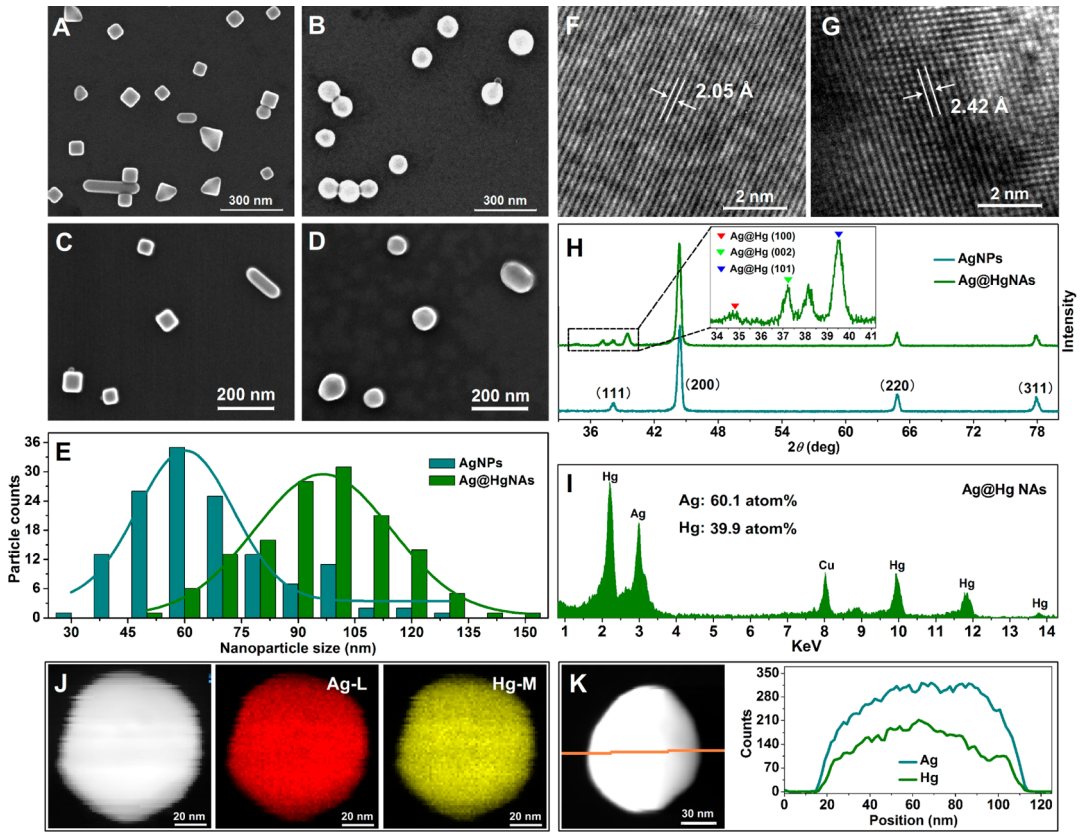

Figure 3. Characterization of the formation of Ag@Hg nanoalloys. (A, B) SEM images; (C, D) SEM images of the same collection of nanoparticles; (F, G) representative HRTEM images; (E) size histograms; (H) XRD of Ag nanoparticles (A, C, F) and the formed Ag@Hg nanoalloys (B, D, G); (I) EDX spectrum; (J) STEM-HAADF image and corresponding of Ag and Hg elemental maps of a Ag@Hg nanoalloy; and (K) STEM-HAADF image of a Ag@Hg nanoalloy and corresponding EDX line profile obtained along the line.

tips and edges of the Ag nanorods, nanocubes, and triangular bipyramids because the active sites mainly belong to the tips and edges of these nanostructures, where the shielding effect of poly(vinyl pyrrolidone) (PVP) did not exist.[9−11] Therefore, amalgamation decreased the effective aspect ratio of the nanorods and rounded the corners and edges of nanocubes and triangular bipyramids. Moreover, the comparison of the same nanoparticles before and after growth further confirmed the above-mentioned results (Figures 3C,D and S6). Second, the atom diffusivity of the formed nanoparticles increased after Hg atoms were doped. Hg bulk has a cohesive energy of 0.67 eV, much lower than that of Ag bulk of 2.95 eV. Thus, alloying Hg with Ag destabilized the crystal. Moreover, the diffusivity of Ag atoms in the interfacial region was enhanced by a factor of 5 when the Hg atoms were doped, indicating that the atomic activity of Ag atoms in the interfacial region could be significantly enhanced by doping with low melting point metals.[44] Furthermore, the active Hg atoms have a higher possibility to diffuse into the nanoparticles' interior. Consequently, diffusion of Hg atoms into Ag nanoparticles led to a dramatic structural modification.

The increase in particle size was observed after growth (Figure 3E). Statistically, the prepared Ag nanoparticles had an average size of 71.1 nm; however, treatment with the growth solution increased the average size of the formed nanoalloys to 101.4 nm, 42.6% more than the pure Ag nanoparticles. The increase in size was attributed to the well-known "swelling effect",[44] occurring during the diffusion of Hg atoms and thus increasing the total atoms per nanoparticles. Assuming that the alloying metals have a molar volume identical to that of the pure elements, the increase in size on mercury incorporation was estimated by the following equation:[38,45]

$$\frac{R}{R_0} = \left(1+\frac{V_{m,Hg}X_{Hg}}{V_{m,Ag}X_{Ag}}\right)^{1/3}$$

where R_0 is the initial particle radius of Ag nanoparticles; R is the particle radius of the formed nanoparticles after amalgamation; $V_{m,Hg}$ and $V_{m,Ag}$ are the molar volumes of metal Hg and Ag, and X_{Hg} and X_{Ag} are the mole fractions of Hg and Ag atoms, respectively. For R_0 = 35.5 nm, R = 50.7 nm, and taking $V_{m,Hg}$ = 14.81 cm^3/mol and $V_{m,Ag}$ = 10.3 cm^3/mol, the molar ratio of the formed Ag@Hg nanoalloys was estimated to be X_{Hg}/X_{Ag} = 1.322:1.

HRTEM characterization showed that Ag nanoparticles have a typical lattice spacing of 2.05 Å (Figure 3F),

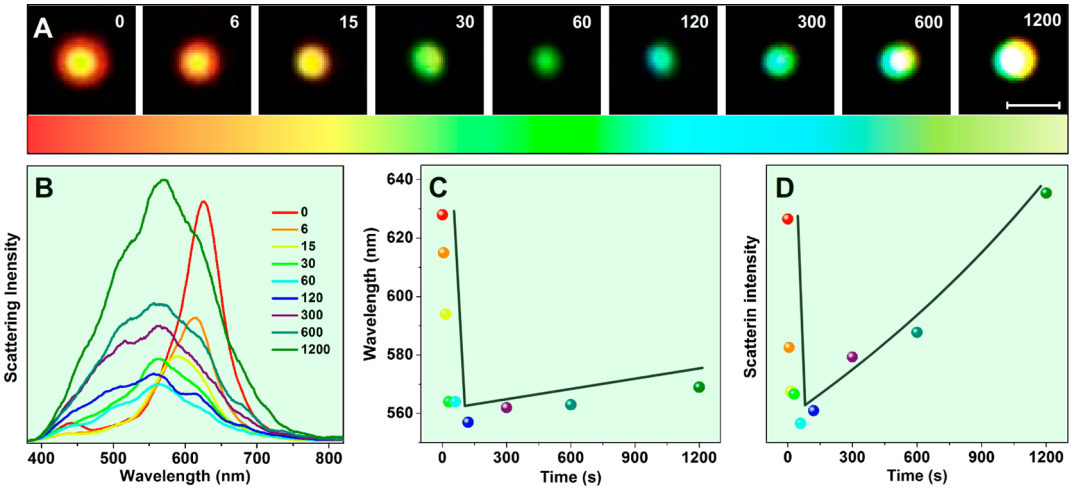

Figure 4. Real-time monitoring of the *in situ* growth of a single Ag@Hg nanoalloy from a Ag nanorod by dark-field scattering microscopy and spectroscopy. (A) Time-dependent dark-field light scattering images and (B) corresponding spectra of a representative Ag nanorod after its exposure to growth solution. (C and D) Scattering wavelength peak and intensity changes of the Ag nanorod as a function of growth time. The color bar in (A) and the lines in (C) and (D) are guides to the eye. The scale bar is 1 μm for all images.

close to the (200) plane of Ag nanoparticles;[46,47] however, the measured lattice spacing of the formed nanoparticles was 2.42 Å (Figure 3G), corresponding to the (002) plane of $Ag_{1.1}@Hg_{0.9}$ nanoalloys.[48] The formed nanoparticles were further analyzed by XRD (Figure 3H). Ag nanoparticles had characterized 2θ peaks at 38.1°, 44.3°, 64.5°, and 77.4°, which are (111), (200), (220), and (311) planes of Ag. Treatment with Hg^0 led to the appearance of new 2θ peaks at about 34.7°, 37.1°, and 39.6° (inset of Figure 3H), corresponding to the (100), (002), and (101) planes of $Ag_{1.1}@Hg_{0.9}$ nanoalloys.[48,49] These results suggested the formation of Ag@Hg nanoalloys, which was confirmed by EDXS analysis. As expected, the formed nanoparticles contained two elements of 60.1 atom % Ag and 39.9 atom % Hg after growth (Figure 3I), effectively proving the formation of Ag@Hg nanoalloys. The signal observed for copper was obtained from the substrate employed in TEM. Additionally, high-angle annular dark-field scanning transmission-electron microscopy (HAADF-STEM) elemental mapping of the formed nanoparticles was performed to reveal the distribution of Ag and Hg elements. Figure 3J showed that Ag and Hg elements were homogeneously distributed in the whole Ag@Hg nanoalloys, which was further confirmed by HAADF-STEM line scanning of a nanoalloy (Figure 3K). These results state that the formed nanoparticles were uniform but not core–shell Ag@Hg nanoalloys and the growth of Ag@Hg nanoalloys followed a mechanism of outside-in diffusion of Hg atoms into Ag nanoparticles.

Monitoring of Single Ag@Hg Nanoalloy Growth. Next, we turn to the real-time monitoring of the *in situ* growth of Ag@Hg nanoalloys. An area containing four typically shaped Ag nanoparticles was selected for real-time observation of the growth of Ag@Hg nanoalloys. Real-time light scattering images constituting the consecutive growth process were taken, and time-dependent spectral information of single Ag nanoparticles was simultaneously acquired to investigate the growth mechanism. Movie S1 displayed the dynamical light scattering images of Ag nanoparticles after their exposure to growth solution. Immediately after the addition of growth solution, almost all Ag nanoparticles exhibited color changes in the scattered light, suggesting the beginning of the growth of Ag@Hg nanoalloys. During the initial stage (within 120 s), noticeable blue-shift of scattered light of single Ag nanoparticles was observed, especially for Ag nanorods (particles 1 and 2). The scattered light of most nanoparticles turned to a weak cyan-green color light that gradually became stronger with prolonged growth time.

For different Ag nanorods (particles 1 and 2 in Movie S1), the scattered light underwent a similar change with different rates. Single Ag nanorods scattered different light at different growth stages. In general, the scattered light turned from red to yellow, green, cyan, and finally to white-yellow (Figure 4A). Further acquired time-dependent single-particle scattering spectra (Figure 4B) showed the following observations. First, the peak wavelength of the nanorod exhibited a noticeable blue-shift from 628 to 557 nm within 120 s followed by a slight red-shift to about 570 nm (Figure 4C), which is consistent with a previous study.[50] Second, the scattering intensity decreased dramatically at early growth stage and then increased with prolonged growth time (Figure 4D). The morphological evolution of Ag nanoparticles during growth was further characterized to explain the LSPR changes. After a treatment of 120 s, almost all Ag nanoparticles turned to spherical Ag@Hg nanoalloys as observed

above. With a prolonged growth time, the particle size of the spherical Ag@Hg nanoalloys increased gradually (Figure S7). Taken together, the above-mentioned observations can be explained as follows: Amalgamation took place more efficiently and preferentially on the tips of the Ag nanorods, as the active sites mainly belong to the tips of the nanorods, and thus decreased the aspect ratios of single Ag nanorods (Figure 3C,D), leading to a blue-shift of the scattered light. At the same time, a significant decrease in aspect ratio reduced the effective size of single Ag nanorods, resulting in weaker scattered light. In addition, although an increase in particle size was seen, the scattered light intensity decreased within 120 s, likely attributed to the smaller scattering cross section of the formed Ag@Hg nanoalloys than that of Ag nanoparticles. Thereafter, diffusion of Hg atoms into Ag nanoparticles gradually increased the particle size (Figure S7), resulting in a slight red-shift of the scattered light and increase in the scattering intensity of Ag@Hg nanoalloys.

Different from rods, the scattered light of Ag triangular bipyramids turned gradually from yellow to green, cyan, and white-yellow (particles 3 and 4 in Movie S1), and no significant change in scattered light color was observed at the early growth stage for Ag nanocubes (particles 5−8 in Movie S1). However, the time-dependent spectral data (Figures S8 and S9) showed that bipyramids and cubes had a similar spectral evolution to that of rods during growth. In addition, the scattered light of Ag nanospheres disappeared at an early growth stage and reappeared and strengthened with prolonged growth time (particles 9 and 10, Movie S1). Due to the disappearance of the scattered light during the growth, the spectral study of single Ag nanospheres was not performed. It is anticipated that amalgamation at the early growth stage rounded the corners and edges of the bipyramids and cubes, resulting in the blue-shift of scattered light. At the same time, the formed nanoalloys had smaller scattering cross section than pure Ag nanoparticles and thus exhibited a decrease or even disappearance of the scattered light. Further Hg^0 diffusion increased the particle size, resulting in the red-shift and increased intensity in scattered light, the same as rods.

Specificity of Hg^0. To demonstrate the specificity of Hg^0 for using this method to produce this kind of nanoalloys, different metals were tested and compared under the same growth conditions. Figure 5A shows the dark-field light scattering images of single Ag nanorods before and after their exposure to growth solution containing different metals. After the growth, only Hg^0 led to a significant scattering change of Ag nanorods, which was further confirmed by scattering spectra (Figure 5B). On exposure to growth solution containing Hg^0 for 30 s, Ag nanorods exhibited a blue-shift of 65 nm as compared to other metals that resulted in insignificant spectral shift (Figure 5C). The

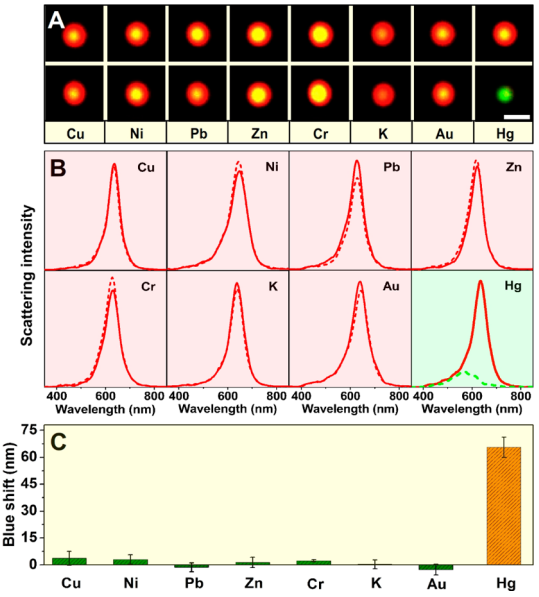

Figure 5. Study of the specificity of Hg^0 in the formation of nanoalloys. (A) Dark-field light scattering images and (B) corresponding resonant scattering spectra of single Ag nanorods before (images above, solid curves) and after (images below, dash curves) their exposure to growth solution for 30 s. (C) Peak wavelength shifts after treatment with different metals. The scale bar is 1 μm for all images.

specificity of Hg^0 was attributed to the much lower cohesive energy of 0.67 eV compared to other metals, such as Cu, Ni, Pb, Zn, Cr, and Au, having cohesive energies of 3.49, 4.44, 2.03, 1.35, 4.10, and 3.81 eV, respectively. Thus, the diffusion of Hg atoms into Ag is much easier than other metals, inducing a change in innate parameters of single Ag nanoparticles. Although K has comparable cohesive energy to Hg^0, it cannot exist in water solution due to the following reaction: $K + H_2O \rightarrow KOH + H_2\uparrow$. In addition, deposition of metal on nanoparticles changes the LSPR scattering property;[35,42,51−53] however no significant change was observed in the experiments employing other metals because the deposition of other metals was not sufficient to create a noticeable change detected by the spectrophotometer.

Mechanism of Ag@Hg Nanoalloy Growth. The aforementioned results showed that the formation of Ag@Hg nanoalloys followed a mechanism of direct amalgamation by the diffusion of Hg atoms into Ag nanoparticles. Figure 6 displays a schematic demonstration of the growth process of Ag@Hg nanoalloys from four typically shaped Ag nanoparticles following a similar process: adsorption of Hg^0 onto Ag nanoparticles occurring on exposure to growth solution followed by rapid diffusion of Hg atoms into Ag nanoparticles and resulting in the formation of bigger spherical Ag@Hg nanoalloys. However, there are some differences between the four typical Ag nanoparticles. For Ag nanospheres, a simple and direct diffusion of Hg atoms in Ag nanospheres occurred after Hg adsorption

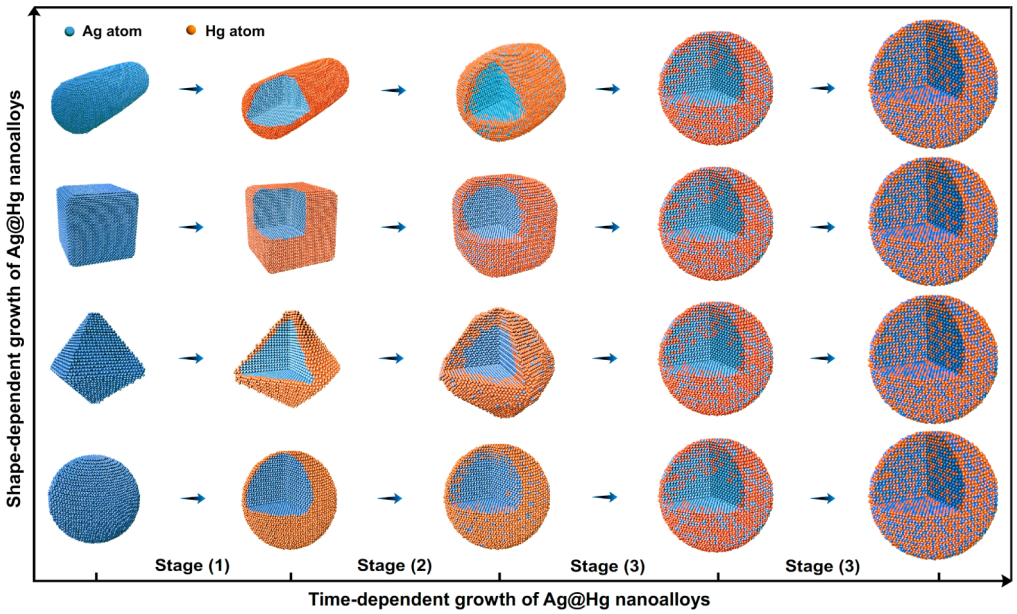

Figure 6. Schematic demonstration of the growth of Ag@Hg nanoalloys from four typical Ag nanoparticles. The following growth stages are involved for all Ag nanoparticles: (1) quick adsorption of Hg atoms onto Ag nanoparticles, (2) early stage diffusion of Hg atoms into Ag nanoparticles, shortening or rounding the particle, (3) further diffusion of Hg atoms and formation of Ag and Hg uniformly distributed spherical Ag@Hg nanoalloys.

led to the formation of Ag@Hg nanoalloys, whereas for Ag nanorods amalgamation occurred preferentially and actively at rod tips at early growth stage and reduced the aspect ratios of Ag nanorods followed by diffusion of Hg atoms to form Ag@Hg nanoalloys. However, for Ag triangular bipyramids and nanocubes, rapid adsorption of Hg^0 onto the tips and edges followed by amalgamation smoothed the nanoparticle corners and edges to form Ag@Hg nanoalloys, and further diffusion of Hg atoms generated spherical Ag@Hg nanoalloys. In all, the growth of Ag@Hg nanoalloys involved amalgamation-induced morphological change at first, and further Hg atom diffusion into Ag nanoparticles resulted in the formation of bigger Ag@Hg nanoalloys with uniform distribution of Ag and Hg elements.

CONCLUSIONS

In summary, real-time monitoring of the *in situ* growth of single Ag@Hg nanoalloys, through direct amalgamation of Ag nanoparticles with Hg^0, using dark-field scattering microscopy was reported. On exposure to growth solution, the scattered light of differently shaped single Ag nanoparticles exhibited a noticeable blue-shift followed by a red-shift. Further characterizations by SEM, HRTEM, XRD, EDXS, and elemental mapping and line scanning confirmed the formation of Ag@Hg nanoalloys. According to the time-dependent spectral data and shape changes of single nanoparticles, the proposed growth mechanism of single Ag@Hg nanoalloys from four typically shaped Ag nanoparticles involved the following stages: first, rapid adsorption of Hg atoms onto Ag nanoparticles; second, early stage diffusion of Hg atoms into Ag nanoparticles, shortening or rounding the particles; third, further diffusion of Hg atoms leading to the formation of Ag and Hg uniformly distributed spherical Ag@Hg nanoalloys. The present work enables us to design Ag@Hg nanoalloys with given optical properties. Especially, nanoalloys scattering a variety of light can be produced by controlling the growth time, and they are expected to be applied for multiple labeling and imaging in biosystems. Furthermore, dark-field scattering microscopy was proven to be a powerful tool for real-time monitoring of the *in situ* growth of single Ag@Hg nanoalloys. Similarly, the growth of other nanoparticles involving Au or Ag nanoparticles or Au@Ag nanoalloys can be monitored by using the methods employed in this study.

EXPERIMENTAL SECTION

Growth of Ag@Hg Nanoalloys. Ag@Hg nanoalloys were grown *in situ* on glass slides by direct exposure of Ag nanoparticles to growth solution as follows: first, Ag nanoparticles were synthesized and chemically attached to previously cleaned and 3-mercaptopropyltrimethoxysilane-treated glass slides following the procedure described in our previous work;[37] second, the Ag nanoparticles-attached glass slides were rinsed with pure water, dried under nitrogen, and placed in the growth solution, containing 1.0×10^{-4} mol/L ascorbic acid and 1.0×10^{-6} mol/L mercury chloride ($HgCl_2$) to form Hg^0, at room temperature to produce Ag@Hg nanoalloys; third, the glass slides were incubated for the designed time as indicated in the text, washed with pure water, dried under nitrogen, and transferred for the following measurements.

Dark-Field Scattering Microscopy. Dark-field light scattering images were captured by a BX51 optical microscope (Olympus, Japan) equipped with a DP72 single chip true-color charge-coupled device (CCD) camera (Olympus, Japan). The white light after crossing a dark-field condenser (U-DCW, 1.2−1.4) excites nanoparticles to scatter colored light, which was collected by a 100× object lens, and dark-field light scattering images were taken by the true-color CCD camera. To real-time monitor the growth of single Ag@Hg nanoalloys, a homemade flow cell (Figure S10) was introduced. An area containing differently shaped Ag nanoparticles was selected for real-time study. After dark-field scattering imaging of initial Ag nanoparticles, growth solution was added into the flow cell to initiate the growth of Ag@Hg nanoalloys. Then, dark-field scattering images of the same area were obtained at different times, as indicated in the text. All the images demonstrate the monitoring of a consecutive growth of single Ag@Hg nanoalloys.

Dark-Field Scattering Spectroscopy. To investigate the spectral properties of single Ag nanoparticles during the growth process in terms of understanding the growth mechanism, single-particle scattering spectra were obtained by dark-field scattering spectroscopy using a spectrograph (MicroSpec-2300i, Roper Scientific) and an intensified CCD camera (PI-MAX, Princeton Instruments) mounted onto the dark-field optical microscope. After image taking and spectral scanning of single representative Ag nanoparticles, the glass slides were placed in a freshly prepared growth solution to initiate the growth. After incubation for a designated time as indicated in the text, the glass slides were washed and dried, and dark-field scattering images of the same nanoparticles were captured with the simultaneous scanning of the scattering spectra. Then, new rounds of growth were performed followed by image taking and spectral scanning until the total growth time was 20 min. In order to achieve co-location of the same nanoparticles after growth and wash every time, a cross label was marked on the glass slides. The bare scattering spectra of single nanoparticles were obtained by selecting a region of the same size where no nanoparticle scattering existed for background subtraction. All scattering spectra of single nanoparticles in this study were smoothed through Origin 8.0 software.

Characterization of Ag@Hg Nanoalloys. The shape and size of Ag nanoparticles during growth were characterized by an S-4800 scanning electron microscope (Hitachi, Japan). Ag@Hg nanoalloys were grown on silicon wafers by the identical method mentioned above. Two experiments with and without including the growth solution were set up to compare the shape and size changes of Ag nanoparticles before and after growth for 20 min. To study the time-dependent morphological evolution, the growth was interrupted at different growth time and SEM images were taken. Further study on the shape changes of four typically shaped Ag nanoparticles was achieved by comparing SEM images of the same nanoparticles before and after growth to understand the growth mechanism. The co-location of the same nanoparticles previously imaged was achieved by marking a cross label on the silicon wafer.

The formation of Ag@Hg nanoalloys was confirmed by HRTEM, XRD, EDXS, HAADF-STEM elemental mapping, and line scan measurements. Before performing TEM measurement, the following processes were required because Ag@Hg nanoalloys grown on glass slides were not suitable for the above measurements. Ag@Hg nanoalloys were collected by sonication of the glass slides for 10 min to remove Ag@Hg nanoalloys from the glass surfaces. The colloidal solution was centrifuged to concentrate Ag@Hg nanoalloys. A drop of concentrated colloidal solution of Ag@Hg nanoalloys was placed onto the carbon film coated copper network, dried at room temperature, and used for further measurements. A Tecnai G2 F20 transmission electron microscope (FEI, America), equipped with an energy-dispersive X-ray spectrometer system and high-angle angular-dark-field detector, was used at 200 kV for high-resolution electron microscopy imaging, composition analysis, and HAADF imaging to study the elemental distribution by achieving elemental mapping and line scanning of Ag@Hg nanoalloys. The probe size for EDXS mapping is less than 1 nm, and the step size about 2 nm. The phase composition of Ag nanoparticles before and after growth was determined with an XRD-7000 X-ray diffractometer (Shimadzu, Japan) using silicon wafers as substrates.

Conflict of Interest: The authors declare no competing financial interest.

Acknowledgment. This work was financially supported by the National Natural Science Foundation of China (NSFC, No. 21035005).

Supporting Information Available: Additional Figures (Figures S1−S10) and Movie S1. This material is available free of charge *via* the Internet at http://pubs.acs.org.

REFERENCES AND NOTES

1. Ferrando, R.; Jellinek, J.; Johnston, R. L. Nanoalloys: From Theory to Applications of Alloy Clusters and Nanoparticles. *Chem. Rev.* **2008**, *108*, 845–910.
2. Cortie, M. B.; McDonagh, A. M. Synthesis and Optical Properties of Hybrid and Alloy Plasmonic Nanoparticles. *Chem. Rev.* **2011**, *111*, 3713–3735.
3. Okabe, T.; Mitchell, R. J. Setting Reactions in Dental Amalgam Part 2. The Kinetics of Amalgamation. *Crit. Rev. Oral Biol. Med.* **1996**, *7*, 23–35.
4. Ojea-Jiménez, I.; López, X.; Arbiol, J.; Puntes, V. Citrate-Coated Gold Nanoparticles as Smart Scavengers for Mercury(II) Removal from Polluted Waters. *ACS Nano* **2012**, *6*, 2253–2260.
5. Lo, S.-I.; Chen, P.-C.; Huang, C.-C.; Chang, H.-T. Gold Nanoparticle−Aluminum Oxide Adsorbent for Efficient Removal of Mercury Species from Natural Waters. *Environ. Sci. Technol.* **2012**, *46*, 2724–2730.
6. Pacheco, S.; Medina, M.; Valencia, F.; Tapia, J. Removal of Inorganic Mercury from Polluted Water Using Structured Nanoparticles. *J. Environ. Eng.* **2006**, *132*, 342–349.
7. Lisha, K. P.; Anshup; Pradeep, T. Towards a Practical Solution for Removing Inorganic Mercury from Drinking Water Using Gold Nanoparticles. *Gold Bull.* **2009**, *42*, 144–152.
8. Sumesh, E.; Bootharaju, M. S.; Anshup; Pradeep, T. A Practical Silver Nanoparticle-Based Adsorbent for the Removal of Hg^{2+} from Water. *J. Hazard. Mater.* **2011**, *189*, 450–457.
9. Rex, M.; Hernandez, F. E.; Campiglia, A. D. Pushing the Limits of Mercury Sensors with Gold Nanorods. *Anal. Chem.* **2006**, *78*, 445–451.
10. Huang, H.; Qu, C.; Liu, X.; Huang, S.; Xu, Z.; Zhu, Y.; Chu, P. K. Amplification of Localized Surface Plasmon Resonance Signals by a Gold Nanorod Assembly and Ultra-Sensitive Detection of Mercury. *Chem. Commun.* **2011**, *47*, 6897–6899.
11. Singh, A.; Pasricha, R.; Sastry, M. Ultra-Low Level Optical Detection of Mercuric Ions Using Biogenic Gold Nanotriangles. *Analyst* **2012**, *137*, 3083–3090.
12. James, J. Z.; Lucas, D.; Koshland, C. P. Gold Nanoparticle Films as Sensitive and Reusable Elemental Mercury Sensors. *Environ. Sci. Technol.* **2012**, *46*, 9557–9562.
13. Deng, L.; Ouyang, X.; Jin, J.; Ma, C.; Jiang, Y.; Zheng, J.; Li, J.; Li, Y.; Tan, W.; Yang, R. Exploiting the Higher Specificity of Silver Amalgamation: Selective Detection of Mercury(II) by Forming Ag/Hg Amalgam. *Anal. Chem.* **2013**, *85*, 8594–8600.
14. Renaud, G.; Lazzari, R.; Revenant, C.; Barbier, A.; Noblet, M.; Ulrich, O.; Leroy, F.; Jupille, J.; Borensztein, Y.; Henry, C. R.; *et al*. Real-Time Monitoring of Growing Nanoparticles. *Science* **2003**, *300*, 1416–1419.
15. Polte, J. R.; Emmerling, F.; Radtke, M.; Reinholz, U.; Riesemeier, H.; Thünemann, A. F. Real-Time Monitoring of Copolymer Stabilized Growing Gold Nanoparticles. *Langmuir* **2010**, *26*, 5889–5894.
16. Abécassis, B.; Testard, F.; Spalla, O.; Barboux, P. Probing *in Situ* the Nucleation and Growth of Gold Nanoparticles by Small-Angle X-Ray Scattering. *Nano Lett.* **2007**, *7*, 1723–1727.

17. Polte, J.; Erler, R.; Thünemann, A. F.; Sokolov, S.; Ahner, T. T.; Rademann, K.; Emmerling, F.; Kraehnert, R. Nucleation and Growth of Gold Nanoparticles Studied *via in Situ* Small Angle X-Ray Scattering at Millisecond Time Resolution. *ACS Nano* **2010**, *4*, 1076–1082.
18. Takesue, M.; Tomura, T.; Yamada, M.; Hata, K.; Kuwamoto, S.; Yonezawa, T. Size of Elementary Clusters and Process Period in Silver Nanoparticle Formation. *J. Am. Chem. Soc.* **2011**, *133*, 14164–14167.
19. Lu, C.; Akey, A. J.; Dahlman, C. J.; Zhang, D.; Herman, I. P. Resolving the Growth of 3D Colloidal Nanoparticle Superlattices by Real-Time Small-Angle X-Ray Scattering. *J. Am. Chem. Soc.* **2012**, *134*, 18732–18738.
20. Peng, S.; Okasinski, J. S.; Almer, J. D.; Ren, Y.; Wang, L.; Yang, W.; Sun, Y. Real-Time Probing of the Synthesis of Colloidal Silver Nanocubes with Time-Resolved High-Energy Synchrotron X-Ray Diffraction. *J. Phys. Chem. C* **2012**, *116*, 11842–11847.
21. Wei, Z.; Zamborini, F. P. Directly Monitoring the Growth of Gold Nanoparticle Seeds into Gold Nanorods. *Langmuir* **2004**, *20*, 11301–11304.
22. Wei, Z.; Qi, H.; Li, M.; Tang, B.; Zhang, Z.; Han, R.; Wang, J.; Zhao, Y. Watching Single Gold Nanorods Grow. *Small* **2012**, *8*, 1331–1335.
23. Ramesh, G. V.; Sreedhar, B.; Radhakrishnan, T. P. Real Time Monitoring of the *in Situ* Growth of Silver Nanoparticles in a Polymer Film under Ambient Conditions. *Phys. Chem. Chem. Phys.* **2009**, *11*, 10059–10063.
24. Senapati, D.; Singh, A. K.; Ray, P. C. Real Time Monitoring of the Shape Evolution of Branched Gold Nanostructure. *Chem. Phys. Lett.* **2010**, *487*, 88–91.
25. Zheng, H.; Smith, R. K.; Jun, Y.-W.; Kisielowski, C.; Dahmen, U.; Alivisatos, A. P. Observation of Single Colloidal Platinum Nanocrystal Growth Trajectories. *Science* **2009**, *324*, 1309–1312.
26. Yuk, J. M.; Park, J.; Ercius, P.; Kim, K.; Hellebusch, D. J.; Crommie, M. F.; Lee, J. Y.; Zettl, A.; Alivisatos, A. P. High-Resolution EM of Colloidal Nanocrystal Growth Using Graphene Liquid Cells. *Science* **2012**, *336*, 61–64.
27. Evans, J. E.; Jungjohann, K. L.; Browning, N. D.; Arslan, I. Controlled Growth of Nanoparticles from Solution with *in Situ* Liquid Transmission Electron Microscopy. *Nano Lett.* **2011**, *11*, 2809–2813.
28. Park, J.; Zheng, H.; Lee, W. C.; Geissler, P. L.; Rabani, E.; Alivisatos, A. P. Direct Observation of Nanoparticle Superlattice Formation by Using Liquid Cell Transmission Electron Microscopy. *ACS Nano* **2012**, *6*, 2078–2085.
29. Yguerabide, J.; Yguerabide, E. E. Light-Scattering Submicroscopic Particles as Highly Fluorescent Analogs and Their Use as Tracer Labels in Clinical and Biological Applications I. Theory. *Anal. Biochem.* **1998**, *262*, 137–156.
30. Burda, C.; Chen, X.; Narayanan, R.; El-Sayed, M. A. Chemistry and Properties of Nanocrystals of Different Shapes. *Chem. Rev.* **2005**, *105*, 1025–1102.
31. Chen, H.; Kou, X.; Yang, Z.; Ni, W.; Wang, J. Shape- and Size-Dependent Refractive Index Sensitivity of Gold Nanoparticles. *Langmuir* **2008**, *24*, 5233–5237.
32. McFarland, A. D.; Van Duyne, R. P. Single Silver Nanoparticles as Real-Time Optical Sensors with Zeptomole Sensitivity. *Nano Lett.* **2003**, *3*, 1057–1062.
33. Becker, J.; Zins, I.; Jakab, A.; Khalavka, Y.; Schubert, O.; Sönnichsen, C. Plasmonic Focusing Reduces Ensemble Linewidth of Silver-Coated Gold Nanorods. *Nano Lett.* **2008**, *8*, 1719–1723.
34. Yang, Y. I.; Jeong, E.; Choi, I.; Lee, S.; Song, H. D.; Kim, K.; Choi, Y.; Kang, T.; Yi, J. Simultaneous Optical Monitoring of the Overgrowth Modes of Individual Asymmetric Hybrid Nanoparticles. *Angew. Chem., Int. Ed.* **2011**, *50*, 4633–4636.
35. Zhang, L.; Li, Y.; Li, D.-W.; Jing, C.; Chen, X.; Lv, M.; Huang, Q.; Long, Y.-T.; Willner, I. Single Gold Nanoparticles as Real-Time Optical Probes for the Detection of NADH-Dependent Intracellular Metabolic Enzymatic Pathways. *Angew. Chem., Int. Ed.* **2011**, *123*, 6921–6924.
36. Skrabalak, S. E.; Au, L.; Li, X.; Xia, Y. Facile Synthesis of Ag Nanocubes and Au Nanocages. *Nat. Protoc.* **2007**, *2*, 2182–2190.
37. Liu, Y.; Huang, C. Z. Screening Sensitive Nanosensors *via* the Investigation of Shape-Dependent Localized Surface Plasmon Resonance of Single Ag Nanoparticles. *Nanoscale* **2013**, *5*, 7458–7466.
38. Mertens, S. F. L.; Gara, M.; Sologubenko, A. S.; Mayer, J.; Szidat, S.; Krämer, K. W.; Jacob, T.; Schiffrin, D. J.; Wandlowski, T. Au@Hg Nanoalloy Formation through Direct Amalgamation: Structural, Spectroscopic, and Computational Evidence for Slow Nanoscale Diffusion. *Adv. Funct. Mater.* **2011**, *21*, 3259–3267.
39. Okabe, T.; Ling, F.-W.; Hochman, R. F. Amalgamation Reaction of Tin, Silver, and Dental Alloy (Ag_3Sn). *J. Biomed. Mater. Res.* **1972**, *6*, 553–563.
40. http://www.knowledgedoor.com/2/elements_handbook/cohesive_energy.html.
41. Qi, W.; Wang, Y.; Wang, J.; Huang, C. Light Scattering Investigations on Mercury Ion Induced Amalgamation of Gold Nanoparticles in Aqueous Medium. *Sci. China Chem.* **2012**, *55*, 1445–1450.
42. Novo, C.; Funston, A. M.; Mulvaney, P. Direct Observation of Chemical Reactions on Single Gold Nanocrystals Using Surface Plasmon Spectroscopy. *Nat. Nanotechnol.* **2008**, *3*, 598–602.
43. Bootharaju, M. S.; Pradeep, T. Investigation into the Reactivity of Unsupported and Supported Ag_7 and Ag_8 Clusters with Toxic Metal Ions. *Langmuir* **2011**, *27*, 8134–8143.
44. Liu, Y.; Zhu, Z.; Liu, G.; Xu, Z.; Kuznicki, S. M.; Zhang, H. A Novel Method to Improve Crystallinity of Supported Nanoparticles Using Low Melting Point Metals. *J. Phys. Chem. C* **2011**, *115*, 14591–14597.
45. Henglein, A.; Giersig, M. Optical and Chemical Observations on Gold−Mercury Nanoparticles in Aqueous Solution. *J. Phys. Chem. B* **2000**, *104*, 5056–5060.
46. Yu, D.; Yam, V. W.-W. Controlled Synthesis of Monodisperse Silver Nanocubes in Water. *J. Am. Chem. Soc.* **2004**, *126*, 13200–13201.
47. Mahmoud, M. A.; El-Sayed, M. A.; Gao, J.; Landman, U. High-Frequency Mechanical Stirring Initiates Anisotropic Growth of Seeds Requisite for Synthesis of Asymmetric Metallic Nanoparticles Like Silver Nanorods. *Nano Lett.* **2013**, *13*, 4739–4745.
48. JCPDS Data File No. [27-0618].
49. Henglein, A.; Brancewicz, C. Absorption Spectra and Reactions of Colloidal Bimetallic Nanoparticles Containing Mercury. *Chem. Mater.* **1997**, *9*, 2164–2167.
50. Bootharaju, M. S.; Chaudhari, K.; Pradeep, T. Real Time Plasmonic Spectroscopy of the Interaction of Hg^{2+} with Single Noble Metal Nanoparticles. *RSC Adv.* **2012**, *2*, 10048–10056.
51. Zheng, X.; Liu, Q.; Jing, C.; Li, Y.; Li, D.; Luo, W.; Wen, Y.; He, Y.; Huang, Q.; Long, Y.-T.; *et al.* Catalytic Gold Nanoparticles for Nanoplasmonic Detection of DNA Hybridization. *Angew. Chem., Int. Ed.* **2011**, *50*, 11994–11998.
52. Choi, I.; Song, H. D.; Lee, S.; Yang, Y. I.; Kang, T.; Yi, J. Core−Satellites Assembly of Silver Nanoparticles on a Single Gold Nanoparticle *via* Metal Ion-Mediated Complex. *J. Am. Chem. Soc.* **2012**, *134*, 12083–12090.
53. Song, H. D.; Choi, I.; Lee, S.; Yang, Y. I.; Kang, T.; Yi, J. On-Chip Colorimetric Detection of Cu^{2+} Ions *via* Density-Controlled Plasmonic Core−Satellites Nanoassembly. *Anal. Chem.* **2013**, *85*, 7980–7986.